Biosensors and Bioelectronics 26 (2011) 4552–4558

Contents lists available at ScienceDirect

Biosensors and Bioelectronics

journal homepage: www.elsevier.com/locate/bios

# Amplified electrochemiluminescence of quantum dots by electrochemically reduced graphene oxide for nanobiosensing of acetylcholine

Shengyuan Deng, Jianping Lei, Lingxiao Cheng, Yangyang Zhang, Huangxian Ju*

*State Key Laboratory of Analytical Chemistry for Life Science, Department of Chemistry, Nanjing University, Nanjing 210093, PR China*

ARTICLE INFO

*Article history:*
Received 18 February 2011
Received in revised form 8 May 2011
Accepted 12 May 2011
Available online 19 May 2011

*Keywords:*
Graphene
Electrochemical reduction
Electrochemiluminescence
Quantum dots
Biosensing
Acetylcholine

ABSTRACT

A signal amplification system for electrochemiluminescence (ECL) of quantum dots (QDs) was developed by using electrochemically reduced graphene oxide (ERGO) to construct a nanobiosensing platform. Due to the structural defects of GO, the ECL emission of QDs coated on GO modified electrode was significantly quenched. After the electrochemical reduction of GO, the restoration of structural conjugation was observed with spectroscopic, morphologic and impedance techniques. Thus in the presence of dissolved $O_2$ as coreactant, the QDs/ERGO modified electrode showed ECL intensity increase by 4.2 and 178.9 times as compared with intrinsic QDs and QDs/GO modified electrodes due to the adsorption of dissolved $O_2$ on ERGO and the facilitated electron transfer. After choline oxidase (ChO) or ChO–acetylcholinesterase was further covalently cross-linked on the QDs/ERGO modified electrode, two ECL biosensors for choline and acetylcholine were fabricated, which showed the linear response ranges and detection limits of 10–210 μM and 8.8 μM for choline, and 10–250 μM and 4.7 μM for acetylcholine, respectively. This green and facile approach to prepare graphene–QDs system could be of potential applications in electronic device and bioanalysis.



## 1. Introduction

Graphene has exhibited tremendous promise in fabricating various nano/mirco-devices such as fuel cells (Guo et al., 2010), solar cells (Cao et al., 2009; Geng et al., 2010), supercapacitors (Segal, 2009), catalysts (Song et al., 2010), biosensors (Shan et al., 2009; Du et al., 2010) and so on. Some methods including micromechanical exfoliation, epitaxial growth by vacuum deposition and chemical conversion (Park and Ruo, 2009) have been developed for preparation of graphene in large scale and high quality to accelerate these utilities (Kim et al., 2009; Bae et al., 2010). Although the micromechanical cleavage approach has led to the discovery of graphene sheets, the low productivity and high cost make it unsuitable for large-scale utilizations. Chemical conversion, performed by oxidizing and sonicating flake graphite to obtain graphene oxide (GO) (Li and Wu, 2009; Liu et al., 2010a) followed with reduction by reducing agent, offers the advantages of synthesis and processing of bulk-quantity graphene nanosheets with low cost, but the use of highly toxic and dangerously unstable $NaBH_4$ or hydrazine to reduce GO requires great care (Zhu et al., 2010). Another challenge is the tendency of irreversible aggregation of the product or restacking into graphite through van der Waals interaction during the chemical reduction. Although it has been overcome by the attachment of polymers onto the nanosheets, the presence of foreign stabilizers is generally undesirable for most applications (Stankovich et al., 2006). Moreover, the reduced graphene sheets remain some oxygenated species derived from the oxidation procedure, which degrades the conductivity and electron mobility, and thus impacts their applications (Guo et al., 2009). Therefore, exploring a more convenient, efficient and environment-friendly approach to produce reduced GO remains a great challenge.

The electrochemical reduction of the exfoliated GO has been proved to be a green and facile way to synthesize large-scale graphene film in high quality due to the intrinsic graphene structure (Wang et al., 2009c; Zhou et al., 2009). No toxic solvent or strong reductant is required during this reduction process, ensuring little contamination of the product. Moreover, the electrical conductivity of the electrochemically reduced graphene oxide (ERGO) is around 8 orders of magnitude larger than those of GO film (Zhou et al., 2009). Despite such distinguished advantages of ERGO, the potential applications have not been explored yet. This work employed ERGO as a supporting material to anchor quantum dots (QDs) and developed an efficient sensitizing method for amplifying the electrochemiluminescent (ECL) emission of QDs and preparing sensitive ECL biosensors.

The combination of graphene and QDs has shown the promising optoelectronic and luminescent properties (Geim, 2009; Kim et al., 2010; Shao et al., 2010). For example, a picoseconds

* Corresponding author. Tel.: +86 25 83593593; fax: +86 25 83593593.
*E-mail address:* hxju@nju.edu.cn (H. Ju).

0956-5663/$ – see front matter © 2011 Elsevier B.V. All rights reserved.
doi:10.1016/j.bios.2011.05.023

ultrafast electron transfer process between the excited QDs and the graphene sheet has been detected by time-resolved fluorescence spectroscopy (Cao et al., 2009), and the anodic ECL of QDs has been amplified by GO in homogeneous aqueous solution (Wang et al., 2009b). Here, the presence of GO on the electrode surface greatly quenched the cathodic ECL emission of immobilized QDs due to its structural defect and low electrical conductivity, which was different from the amplified anodic ECL of QDs. Upon the electrochemical reduction of GO, however, the ECL emission was remarkably improved. ERGO showed obvious ECL sensitization by enhancing the electron transfer and the strong adsorption of dissolved $O_2$. The amplified ECL emission thus provided an avenue for extending the application of ERGO in bioanalysis.

In view of the importance of choline and acetylcholine detection in normal and pathological physiology (Zhao et al., 2008), many acetylcholinesterase (AChE) and choline oxidase (ChO)-based sensors for choline and acetylcholine via ECL (Wang et al., 2009a), amperometric (Wang et al., 2006; Helia et al., 2009; Tan and Lowe, 2009) and fluorescent measurements have been proposed (Vamvakaki et al., 2008). This work used AChE and ChO enzymatic reactions to validate the extended application of the amplified ECL emission by covalently cross-linking these enzymes on the QDs/ERGO modified electrode. The enzymatic reactions consumed the dissolved $O_2$, thus decreasing the ECL signal upon addition of the substrate. The two fabricated ECL biosensors showed fast ECL responses to acetylcholine and choline with acceptable sensitivity. The ERGO exhibited a practical application for constructing sensitive QD-based ECL biosensors.

## 2. Experimental

### 2.1. Reagents and apparatus

Cadmium chloride ($CdCl_2{\cdot}2.5H_2O$), meso-2,3-dimercaptosuccinic acid (DMSA) and glutaraldehyde (GLD, 25% aqueous solution) were purchased from Alfa Aesar China Ltd. Acetylcholinesterase (E.C. 232-559-3, 425.94 U/mg solid), choline oxidase (E.C. 232-840-0, 12.5 U/mg solid), and choline chloride were purchased from Sigma Chemical Co. (St. Louis, MO). Graphite and acetylcholine chloride were purchased from Sinopharm Chemical Reagent Co., Ltd. Te rod (4 mm in diameter) was purchased from Leshan Kayada Photoelectricity Co., China. 0.1 M pH 7.0 phosphate buffer (PBS) was prepared by mixing the stock solutions of $NaH_2PO_4$ and $Na_2HPO_4$ with 0.1 M $KNO_3$ as the supporting electrolyte. Other reagents were of analytical grade and used as received. The ultrapure water (≥18 MΩ, Milli-Q, Millipore) was used throughout the work.

X-ray photoelectron spectral (XPS) experiments were operated on a K-Alpha X-ray photoelectron spectrometer (Thermo Fisher Scientific Co., USA). UV–vis solid-state diffuse reflection (SDR) spectra were obtained on a Shimadzu UV-3600 UV–vis-NIR photospectrometer (Shimadzu Co., Japan). Photoluminescence (PL) spectra were obtained on a RF-5301 PC fluorometer (Shimadzu Co., Japan). After coated with Pt film, the morphologies of sample films were examined under a Hitachi S-4800 scanning electron microscope (SEM, Hitachi, Japan). Transmission electron microscopic (TEM) images were obtained on JEM-2100 (Japan). The static water contact angles were measured at 25 °C by a contact angle meter (Rame-Hart-100) employing drops of deionized water. Tapping mode atomic force microscopic (AFM) images were acquired under ambient conditions by using an Agilent 5500 AFM/SPM system. Electrochemical impedance spectroscopic (EIS) analysis was performed with an Autolab PGSTAT12 (Ecochemie, BV, The Netherlands) in 5 mM $K_3Fe(CN)_6/K_4Fe(CN)_6$ with 0.1 M KCl as the supporting electrolyte. Cyclic voltammetric (CV) and ECL measurements were carried out on a MPI-E multifunctional electrochemical and chemiluminescent analytical system (Xi'an, China) at room temperature with the modified glassy carbon electrode (GCE, 5 mm in diameter, China) as working, a platinum wire as counter and a Ag/AgCl (saturated KCl) as reference electrodes. The emission window was placed in front of the photomultiplier tube biased at 800 V.

### 2.2. Preparation of GO and ERGO

GO was synthesized from graphite by the modified Hummers method (Li and Wu, 2009; Liu et al., 2010a). The as-synthesized graphite oxide was suspended in water and subjected to dialysis for one week to remove residual salts. After dried at 50 °C overnight, as-purified graphite oxide was exfoliated into GO by ultrasonicating a 0.05 wt% aqueous dispersion for 30 min. Unexfoliated graphite oxide was removed by a 5 min ultrafiltration at 2000 rcf. ERGO was acquired by scanning the GO/GCE between 0 and −1.2 V for 50 cycles in pH 7.0 PBS. The as-prepared ERGO film was detached from the electrode by gentle rinse, smashed and sonicated into a near homogeneous dispersion.

### 2.3. Preparation of QDs

The synthesis of CdTe QDs was referred to a green method (Ge et al., 2008) using Te rod as working electrode and DMSA as stabilizer under $N_2$ atmosphere. The resulting solution was refluxed at 80 °C for 20 h to obtain DMSA-CdTe QDs. Before modification, QDs solution was mixed with isopropyl alcohol and centrifuged at 8000 rpm. The precipitation was then dissolved in deionized water with a concentration of 7.6 μM.

### 2.4. Fabrication of ECL biosensors

The GCE was polished successively with 1.0 and 0.05 μm alumina slurry (Beuhler). After successive sonication in acetone and deionized water, the electrode was dried under $N_2$. 20 μL of 0.1 mg/mL GO dispersion was spread on a pretreated bare GCE. The electrode was dried in a silica gel desiccator at room temperature. After the electrochemical reduction of GO, 15 μL of 7.6 μM QDs solution was dropped onto ERGO film and dried in air. 10 μL of 250 U/mL AChE and/or 10 μL of 122.5 U/mL ChO, both prepared in 0.01 M pH 7.0 PBS, were covered on the modified layer and dried at 4 °C. Finally, the enzymes were cross-linked by GLD by vapor-bathing for 10 min to fabricate a stable AChE–ChO/QDs/ERGO/GCE or ChO/QDs/ERGO/GCE. The biosensor was stored in 0.1 M pH 7.0 PBS in 4 °C refrigerator when not in use.

## 3. Results and discussion

### 3.1. Structural and morphology characterization of GO and ERGO

The differences in the elemental composition and structure of GO and ERGO were characterized by XPS. The C 1s XPS spectrum of GO (Fig. 1A) clearly indicated a considerable degree of oxidation with three different O-functionalities assigned to C–O at 287.1 eV, C=O at 288.5 eV, and O–C=O at 289.6 eV (Stankovich et al., 2007). In the C 1s XPS spectrum of ERGO (Fig. 1B), the C–C peak at 284.8 eV became dominant. Moreover, ERGO film exhibited a much lower O/C ratio of 6.45% compared with GO film of 80.63%, indicating a successfully deoxygenating electroreduction process.

The electrochemical reduction of GO was also monitored by UV–vis SDR and PL spectra. GO showed an absorption peak at 228 nm (Fig. 1C, curve b), which originated from the π-plasmon transition of aromatic $sp^2$ domains. After electrochemical reduction, the absorption peak red-shifted to 262 nm (Fig. 1C, curve

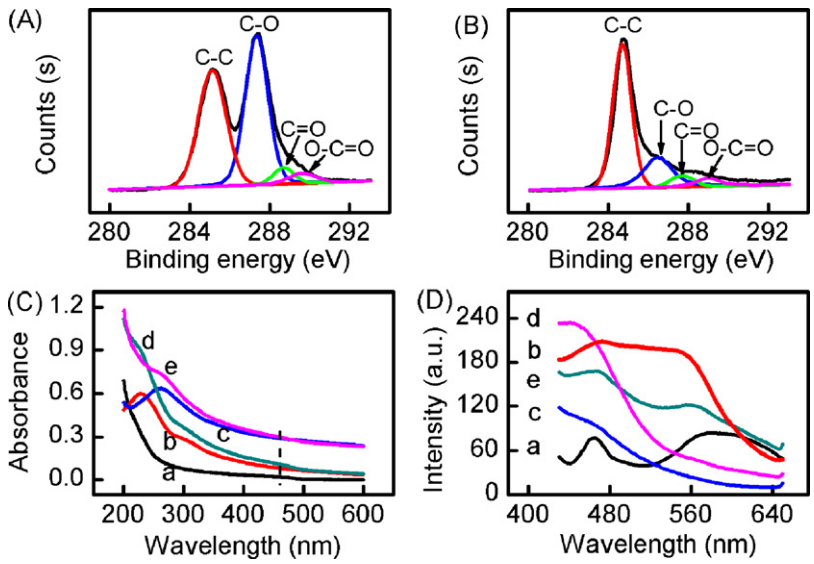


**Fig. 1.** C 1s XPS spectra of (A) GO and (B) ERGO, and (C) UV–vis SDR and (D) PL spectra of QDs (a), GO (b), ERGO (c), QDs/GO (d) and QDs/ERGO (e).

c), indicating restoration of the electronic conjugation. The significant hyperchromicity in the visible and near-infrared range upon the reduction led to the color change from yellow brown to black, also suggesting that the electroreduction released local strain of GO induced by the O-species and increased conjugation in graphene sheets (Stankovich et al., 2007). The UV–vis spectrum of QDs showed a wide absorption band with an absorption inflection point at 461 nm (Fig. 1C, curve a). In the presence of QDs, both absorption peaks of GO and ERGO slightly red-shifted (Fig. 1C, curves d and e), which was similar to the phenomenon observed previously (Geng et al., 2010).

The PL spectrum of QDs showed two emission peaks at 464 and 588 nm (Fig. 1D, curve a). The emission peak at shorter wavelength was consistent with the UV–vis absorption inflection point, indicating the band gap emission of the core. Meanwhile, the emission peak at longer wavelength was attributed to the surface trap emission, which usually shows red-shift by hundreds of nanometers compared to the PL emission from the core (Liu et al., 2010b). GO exhibited an excitation-dependent PL behavior like other luminescent carbon nanoparticles (Pan et al., 2010). At an excitation wavelength of 350 nm, the PL spectrum of GO showed two emission peaks at 465 and 556 nm (Fig. 1D, curve b), the latter vanished as GO was converted into ERGO (Fig. 1D, curve c), indicating the luminescent species were surface defects derived from various O-functionalities on GO sheets (Fan et al., 2009; Pan et al., 2010). Electroreduction restored the structural conjugation, resulting in the disappearance of PL emission. The wavelengths corresponding to the PL emission peaks of QDs approximated those of GO, indicating the Fermi level of GO overlapped with the band gap of QDs. So when QDs and GO coexisted, the fluorescence of CdTe QDs was quenched by GO nanosheets (Fig. 1D, curve d). Contrarily, QDs/ERGO remained the PL emission peak of QDs at 556 nm (Fig. 1D, curve e), further indicating the restoration of the structural conjugation of graphene nanosheets.

SEM image revealed that ERGO film consisted of randomly thin, aggregated and crumpled sheets, which closely associated with each other to form a disordered solid surface (Fig. 2A). Its bright-field TEM image exhibited silk veil-liked waves (Fig. 2B) with a very stable nature under the electron beam (Carlsson, 2007). Different from the chemical reduction of GO which led to the aggregation or restack of graphene nanosheets into graphite (Li et al., 2008), the electrochemical reduction of GO showed barely aggregation, indicating that the assembly of GO sheets on a solid substrate was a good way to prevent the aggregation of reduced GO. The SEM image showed rough and open structure of AChE–ChO/QDs/ERGO (Fig. 2D), which was obviously different from the morphology of QDs/ERGO (Fig. 2C), and made the substrate easily access to the enzyme molecules.

The contact angles of the bare ITO, GO and ERGO films were measured to be 72.2°, 40.5° and 59.6° (Fig. 3A–C), respectively. The higher contact angle of ERGO film than GO indicated less hydrophilic, which was contributed to the decrease of O-functionalites such as carbonyl and carboxylic groups during the electrochemical reduction. AFM image of ERGO film (Fig. 3D) showed an aggregated and crumpled surface with large area, which was similar to Fig. 2A and B. However, the topograph of ERGO film was quite different from that of GO (Fig. 3E), which dispersed in small flakes due to structural defects and electrostatic repulsions among each other. While the average thickness of GO was measured to be 1.1 nm arising from covalently bound O-functionalites, ERGO film with an average thickness of 20 nm was thicker due to the intrinsic out-of-plane deformation as well as sheet-to-sheet overlapping during the electroreduction of GO into ERGO.

From the Nyquist plots obtained in the frequency range from $10^{-1}$ to $10^{5}$ Hz, the bare GCE showed an electron transfer resistance ($R_{ct}$) of about 210 Ω (Fig. 4A, curve a), while the $R_{ct}$ value of GO modified GCE was 550 Ω (Fig. 4A, curve b). After electrochemical reduction, the resistance of the ERGO modified GCE dropped dramatically to 94 Ω (Fig. 4A, curve c), proving that ERGO could accelerate heterogeneous electron transfer between the electroactive species and electrode. The QDs showed a $R_{ct}$ value of around 2050 Ω (Fig. 4A, curve d); and the value further raised to ~3600 Ω after QDs was immobilized on GO modified GCE due to the low conductivity and mobility of GO (Fig. 4A, curve e). However, after the GO was electrochemically reduced, the electron transfer rate greatly increased, and the $R_{ct}$ value at CdTe QDs/ERGO/GCE was 140 Ω (Fig. 4A, curve f), indicating that the presence of ERGO enhanced the electron transfer between the redox probe and the electrode.

### 3.2. Electrochemical reduction of GO and ECL of QDs on ERGO film

Two electrochemical techniques can be employed for preparation of ERGO film: the potential step methods like CV and differential potential voltammetry (Guo et al., 2009; Wang et al.,

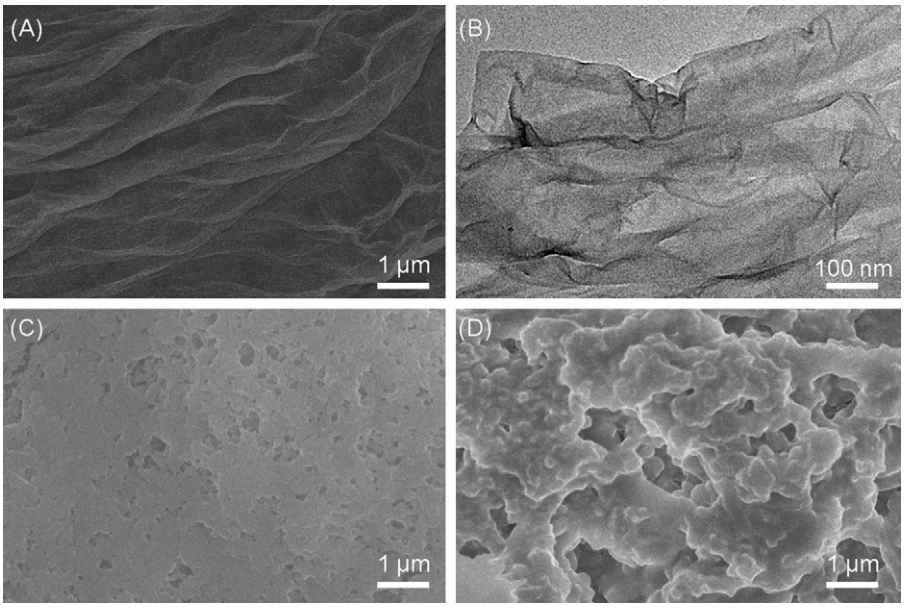


**Fig. 2.** (A) SEM and (B) TEM images of ERGO, SEM images of (C) QDs/ERGO and (D) AChE–ChO/QDs/ERGO.

2009c) and the potentiostatic techniques like chronoamperometry (Zhou et al., 2009). Here CV was chosen for electrochemical reduction of GO by scanning the potential between 0 and −1.2 V. The cyclic voltammogram of GO modified electrode showed the increasing cathodic current beyond −0.85 V (Fig. 4B). This large reduction current should be due to the reduction of the surface oxygenated functional groups since the reduction of water to hydrogen occurred at more negative potentials (*e.g.*, −1.5 V). Interestingly, the reduction current decreased gradually and disappeared after several potential scans. This demonstrated that the reduction rate of surface-oxygenated species at GO occurred quickly and irreversibly. The electrochemical reduction mechanism of GO could be explained with the model of three-phase interlines (Zhou et al., 2009). As the pH increased, the reduction peak potentials of GO shifted negatively with a slope of $-71\,\mathrm{mV\,pH^{-1}}$, indicating the reduction process required the participation of protons. As the electrochemical reaction proceeded, a black area could be directly observed on electrode surface. The color change could be attributed to the GO reduction and the π network restoration within the carbon structure of the obtained ERGO film, which had been witnessed during the chemical reduction of GO (Zhou et al., 2009). These dynamic changes indicated the structure of graphene was restored during the reduction.

In air-saturated PBS the ECL emission of QDs/ERGO modified GCE could be greatly improved as compared with intrinsic QDs modified GCE. The ECL peak intensity of QDs/ERGO/GCE at −1.05 V was 9128 (Fig. 4C, curve a), while the peak intensity of QDs/GCE was 2128 (Fig. 4C, curve c), indicating an improvement by 4.2 times. At QDs/GO/GCE the ECL peak intensity was only 51 (Fig. 4D, curve a), indicative of quenching effect of GO on the ECL of QDs, which resulted from the structural defects of GO and its blocking off the electron transfer between QDs and the electrode. The electrochemical reduction of GO to ERGO could produce a 178.9 times enhancement of ECL intensity.

Since no obvious ECL emission could be observed at bare GCE, GO and ERGO modified GCEs, the ECL emission should be pro-

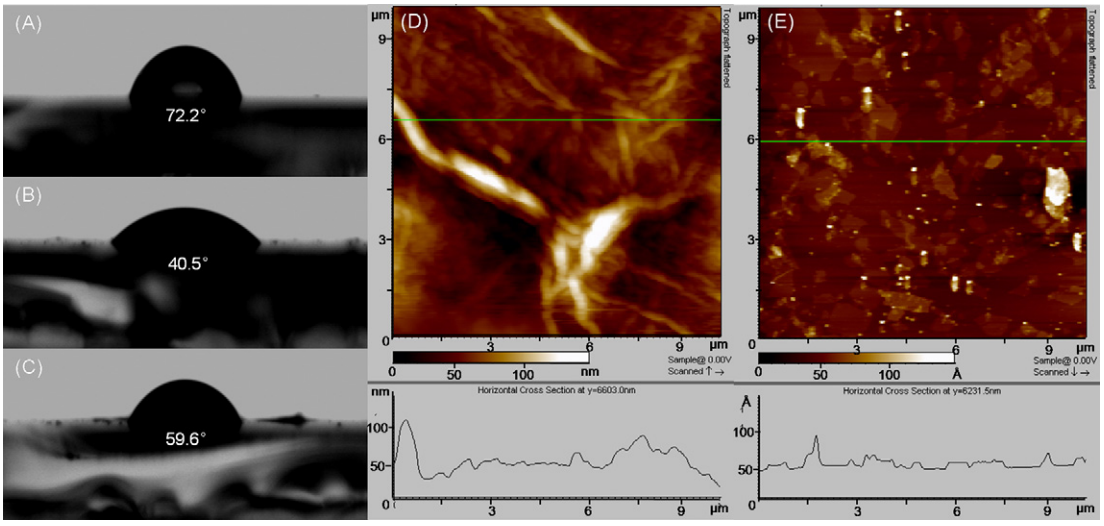


**Fig. 3.** Contact angle photographs of (A) bare, (B) GO and (C) ERGO modified ITO slides, and AFM images and height profiles of (D) ERGO and (E) GO.

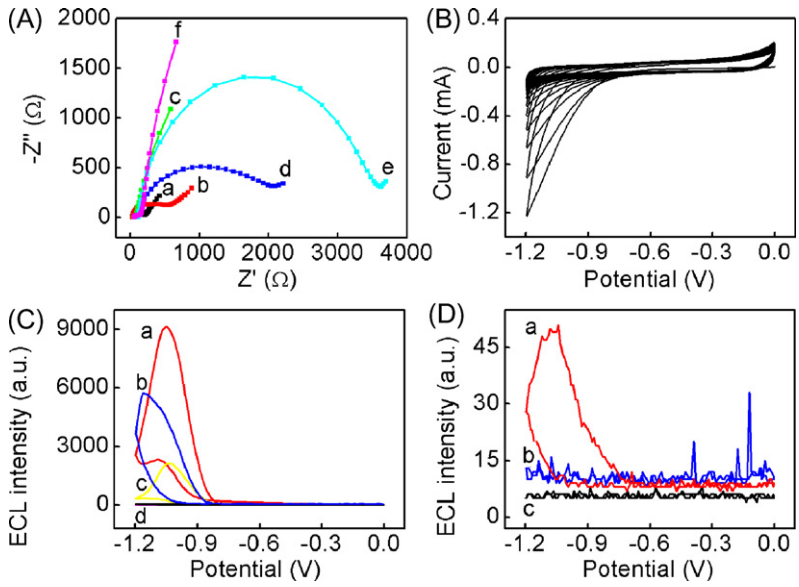


**Fig. 4.** (A) EIS Nyquist plots of bare GCE (a), GO/GCE (b), ERGO/GCE (c), QDs/GCE (d), QDs/GO/GCE (e), and QDs/ERGO/GCE (f). (B) Cyclic voltammogram of GO/GCE in $N_2$-saturated PBS at a scan rate of 100 mV/s. (C) ECL-potential curves of QDs/ERGO/GCE in air-saturated (a) and $N_2$-saturated (b) PBS, QDs/GCE (c) and bare GCE (d) in air-saturated PBS. (D) QDs/GO/GCE in air-saturated PBS (a), QDs/GCE (b) and bare GCE (c) in $N_2$-saturated PBS.

duced from QDs. According to the previous mechanism (Jiang and Ju, 2007b), the ECL process could be expressed as follows:

$$\mathrm{CdTeQDs} + ne^- \rightarrow n\mathrm{R}^{\bullet -} \quad (1)$$

$$\mathrm{O_2} + 2\mathrm{R}^{\bullet -} + 2\mathrm{H}^+ \rightarrow 2\mathrm{R}^* + \mathrm{H_2O_2} \quad (2)$$

$$\mathrm{H_2O_2} + 2\mathrm{R}^{\bullet -} \rightarrow 2\mathrm{R}^* + 2\mathrm{OH}^- \quad (3)$$

$$\mathrm{Then R}^* \rightarrow \mathrm{R} + h\nu \quad (4)$$

$\mathrm{R}^{\bullet -}$ represented the electron-injected QDs produced during the cathodic scan, while $\mathrm{R}^*$ stood for the excited-state QDs.

It was inferred from Eqs. (2) and (3) that given no introduction of exogenous coreactants like $S_2O_8^{2-}$, the coreactant for ECL emission of QDs was dissolved $O_2$ as well as $H_2O_2$ derived from $O_2$. Therefore, once $N_2$ was bubbled through the solution for a sufficient duration (*i.e.*, 30 min) to eliminate $O_2$, the ECL intensity of QDs would reduce to 0 (Fig. 4D, curve b). However, the ECL peak intensity of QDs/ERGO modified GCE in $N_2$-saturated PBS was 5720 (Fig. 4C, curve b). Thus, the $N_2$ atmosphere did not completely eliminate $O_2$ from the neighborhood area of QDs/ERGO/GCE, and $O_2$ could strongly adsorb on ERGO. This phenomenon indicated the improved ECL emission of QDs resulted from not only the high electronic conductivity of ERGO but also the adsorption of $O_2$ on ERGO. The strong and stable ECL of QDs/ERGO/GCE with the endogenous coreactant dissolved $O_2$ could be desirable to construct the enzyme-based ECL biosensing platform.

### 3.3. Condition optimization

To apply the functional film in biosensing, several experimental parameters including the volume of GO dispersion ($V_{GO}$), the

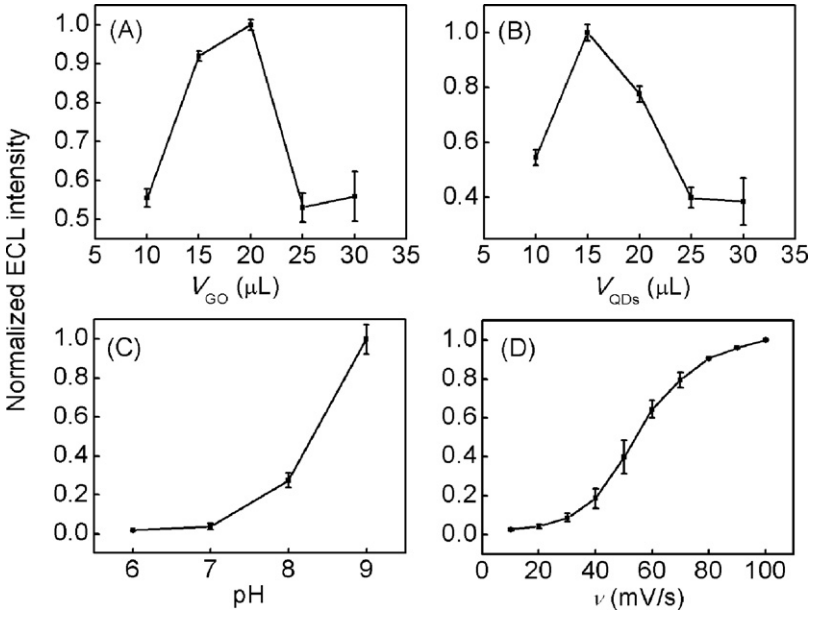


**Fig. 5.** Effects of (A) $V_{GO}$, (B) $V_{QDs}$, (C) pH and (D) $\nu$ on ECL peak intensity of QDs. When one parameter changes, the others are at their optimal values.

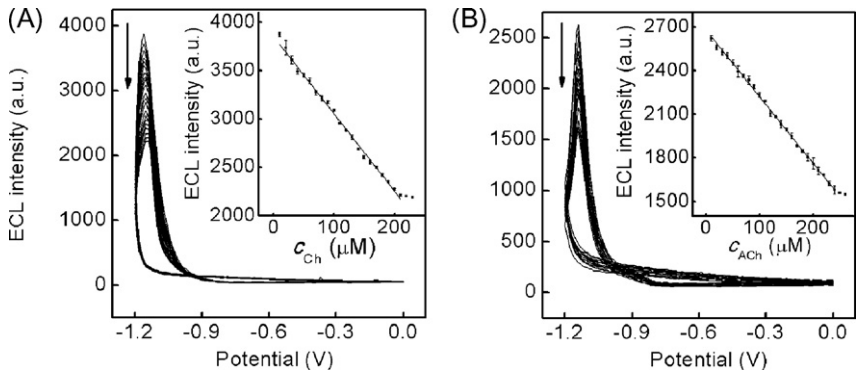


**Fig. 6.** ECL-potential curves of (A) ChO/QDs/ERGO/GCE for choline from 10 to 210 μM with 10 μM increment and (B) AChE–ChO/QDs/ERGO/GCE for acetylcholine from 10 to 250 μM with 20 μM increment in air-saturated PBS. Inset: calibration curves.

amount of QDs deposited ($V_{QDs}$), the solution pH and potential scan rate ($\nu$) were optimized. The ECL peak intensity enhanced steadily as $V_{GO}$ grew up to 20 μL (Fig. 5A), which indicated that the more condensed state of ERGO would more efficiently facilitate the generation of the electron-injected QDs. However, the ECL peak intensity decreased dramatically with $V_{GO}$ over 20 μL. It has reported that carbon nanomaterials can absorb light as a blackbody (Wang et al., 2009a). Thus $V_{GO}$ for electrochemically reduction was chosen to be 20 μL.

The quantity of the excited state $R^*$ essentially depended on $V_{QDs}$. With an increasing QDs density, the formed individual nanocrystal species increased during the cathodic scan, leading to enhancement in ECL intensity (Fig. 5B). The strongest ECL intensity was obtained at 15 μL of QDs solution modified GCE, consistent with the close-packed structure of QDs (Fig. 2C). As $V_{QDs}$ exceeded 15 μL, the ECL intensity decreased, which indicated that the overloaded QDs increased the film thickness and inhibited the electron exchange with radical species.

The ECL emission of QDs also related to the pH value of detection solution. As shown in Fig. 5C, the ECL intensity increased with pH changing from 6.0 to 9.0. Considering that a much higher pH value over 9.0 was unfavorable for further application, pH 9.0 PBS was used as the detection solution.

The scan rate could affect the ECL over a wide range, since the ECL efficiency significantly depended on the rate of generation/annihilation of $R^*$ (Jiang and Ju, 2007b). High scan rate could enrich $R^*$ in a short time span enhancing ECL intensity (Fig. 5D). The ECL intensity increased with the increasing scan rate and kept steadily at 80 mV/s, indicating the emitted photons came to saturation.

### 3.4. ECL enzyme-based biosensors

Under optimized conditions, AChE–ChO/QDs/ERGO/GCE showed strong and stable ECL signal (Fig. 6). Upon addition of acetylcholine, the AChE catalyzed its hydrolysis to produce choline, which was oxidized by dissolved $O_2$ with the help of ChO. The consumption of coreactant decreased the ECL signal (Fig. 6). The decrease of ECL signal was proportional to the concentration of acetylcholine in a range of 10–250 μM with a quenching constant of $4.6 \times 10^6\ M^{-1}$. The detection limit was 4.7 μM (S/N = 3). Similarly, the ChO/QDs/ERGO/GCE showed the linear range of 10–210 μM for choline with a quenching constant of $8.0 \times 10^6\ M^{-1}$ and a detection limit of 8.8 μM (S/N = 3). Both the quenching constants were larger than $1.4 \times 10^6\ M^{-1}$ for acetylcholine and $9.7 \times 10^5\ M^{-1}$ for choline at carbon nanotubes enhanced CdS QDs ECL biosensor (Wang et al., 2009a), indicating more sensitive response of QDs/ERGO/GCE to the analytes. The proposed biosensors also showed higher sensitivity than the amperometric biosensors for acetylcholine with a linear range of 1.5–12.5 mM and detection limit of ~0.01 mM (Tan and Lowe, 2009), a linear range of 20–2680 μM and detection limit of 39 μM (Helia et al., 2009) and a detection limit of 0.10 mM (Pchelintsev and Millner, 2008), and the amperometric biosensor for choline with a linear range of 50–5000 μM and detection limit of 10 μM (Wang et al., 2006).

The stability of biosensors for choline and acetylcholine was examined by measuring their ECL responses after storage in PBS at 4 °C for 7 days. The ECL responses of the two biosensors to 100 μM substrates did not show obvious decline, demonstrating good stability. The reproducibility of the biosensors was investigated by detecting 100 μM analytes. The intra-assay relative standard deviations (RSDs) for choline and acetylcholine were evaluated by thrice measurements to be 4.5% and 6.1%, respectively; and the inter-assay RSDs for choline and acetylcholine were estimated with five biosensors fabricated independently to be 7.2% and 8.8%, respectively, showing acceptable fabrication reproducibility of the two ECL biosensors. The concentration of acetylcholine in the extracellular fluid of the brain is 0.1–6 nM (Nirogi et al., 2010). By combining with a preconcentration step, the proposed ECL biosensors could be potentially applied to monitor the important neurotransmitter during normal or altered pathological conditions.

## 4. Conclusion

A graphene-amplified solid-state ECL biosensing platform was successfully constructed by immobilizing QDs on ERGO. ERGO could be quickly prepared by direct electrochemical reduction of GO. The reduction process efficiently restored the backbone structure of graphene, enhanced the electronic conjugation in graphene sheets, and produced new graphitic domains with smaller size, which led to high electronic conductivity and strong adsorption of $O_2$ on ERGO. Thus ERGO could greatly enhance the ECL emission of QDs when using $O_2$ as the coreactant. The amplified ECL of QDs/ERGO could be used to construct sensitive biosensors based on the consumption of dissolved $O_2$ in enzymatic reaction. Two ECL biosensors for choline and acetylcholine were successfully prepared by covalently cross-linking ChO and AChE–ChO on QDs/ERGO/GCE. The good performance of the biosensors indicated that the ERGO could be of potential applications with convenient and high quality production.

## Acknowledgements

This research was financially supported by the Important National S&T Specific Project (2009ZX10004-313), National Basic

Research Program of China (2010CB732400) and National Natural Science Foundation of China (20821063 and 20875044).

## References


Bae, S., Kim, H., Lee, Y., Xu, X.F., Park, J.S., Zheng, Y., Balakrishnan, J., Lei, T., Kim, H.R., Song, Y.I., Kim, Y.J., Kim, K.S., Özyilmaz, B., Ahn, J.H., Hong, B.H., Iijima, S., 2010. Nat. Nanotechnol. 5, 574–578.

Cao, A.N., Liu, Z., Chu, S.S., Wu, M.H., Ye, Z.M., Cai, Z.W., Chang, Y.L., Wang, S.F., Gong, Q.H., Liu, Y.F., 2009. Adv. Mater. 21, 1–4.

Carlsson, J.M., 2007. Nat. Mater. 6, 801–802.

Du, D., Zou, Z.X., Shin, Y.S., Wang, J., Wu, H., Engelhard, M.H., Liu, J., Aksay, I.A., Lin, Y.H., 2010. Anal. Chem. 82, 2989–2995.

Fan, F.R.F., Park, S.J., Zhu, Y.W., Ruoff, R.S., Bard, A.J., 2009. J. Am. Chem. Soc. 131, 937–939.

Ge, C.W., Xu, M., Liu, J., Lei, J.P., Ju, H.X., 2008. Chem. Commun. 44, 450–452.

Geim, A.K., 2009. Science 324, 1530–1534.

Geng, X.M., Niu, L., Xing, Z.Y., Song, R.S., Liu, G.T., Sun, M.T., Cheng, G.S., Zhong, H.J., Liu, Z.H., Zhang, Z.J., Sun, L.F., Xu, H.X., Lu, L., Liu, L.W., 2010. Adv. Mater. 22, 638–642.

Guo, H.L., Wang, X.F., Qian, Q.Y., Wang, F.B., Xia, X.H., 2009. ACS Nano 3, 2653–2659.

Guo, S.J., Dong, S.J., Wang, E.K., 2010. ACS Nano 4, 547–555.

Helia, H., Hajjizadehb, M., Jabbarib, A., Moosavi-Movahedi, A.A., 2009. Biosens. Bioelectron. 24, 2328–2333.

Jiang, H., Ju, H.X., 2007b. Chem. Commun. 43, 404–406.

Kim, K.S., Zhao, Y., Jang, H., Lee, S.Y., Kim, J.M., Kim, K.S., Ahn, J.H., Kim, P., Choi, J.Y., Hong, B.H., 2009. Nature 457, 706–710.

Kim, Y.T., Han, J.H., Hong, B.H., Kwon, Y.U., 2010. Adv. Mater. 22, 515–518.

Li, Y.G., Wu, Y.Y., 2009. J. Am. Chem. Soc. 131, 5851–5857.

Li, D., Müller, M.B., Gilje, S., Kaner, R.B., Wallace, G.G., 2008. Nat. Nanotechnol. 3, 101–105.

Liu, J.B., Fu, S.H., Yuan, B., Li, Y.L., Deng, Z.X., 2010a. J. Am. Chem. Soc. 132, 7279–7281.

Liu, X., Cheng, L.X., Lei, J.P., Liu, H., Ju, H.X., 2010b. Chem. Eur. J. 16, 10764–10770.

Nirogi, R., Mudigonda, K., Kandihere, V., Ponnamaneni, R., 2010. Biomed. Chromatogr. 1, 39–48.

Pan, D.Y., Zhang, J.C., Li, Z., Wu, M.H., 2010. Adv. Mater. 22, 734–738.

Park, S.J., Ruo, R.S., 2009. Nat. Nanotechnol. 4, 217–224.

Pchelintsev, N.A., Millner, P.A., 2008. Anal. Chim. Acta 612, 190–197.

Segal, M., 2009. Nat. Nanotechnol. 4, 612–614.

Shan, C.S., Yang, H.F., Song, J.F., Han, D.X., Ivaska, A., Niu, L., 2009. Anal. Chem. 81, 2378–2382.

Shao, Y.Y., Wang, J., Wu, H., Liu, J., Aksay, I.A., Lin, Y.H., 2010. Electroanalysis 22, 1027–1036.

Song, Y.J., Qu, K.G., Zhao, C., Ren, J.S., Qu, X.G., 2010. Adv. Mater. 22, 2206–2210.

Stankovich, S., Dikin, D.A., Dommett, G.H.B., Kohlhaas, K.M., Zimney, E.J., Stach, E.A., Piner, R.D., Nguyen, S.B.T., Ruoff, R.S., 2006. Nature 442, 282–286.

Stankovich, S., Dikin, D.A., Piner, R.D., Kohlhaas, K.A., Kleinhammes, A., Jia, Y.Y., Wu, Y., Nguyen, S.B.T., Ruoff, R.S., 2007. Carbon 45, 1558–1565.

Tan, E.V., Lowe, C.R., 2009. Anal. Chem. 81, 7579–7589.

Vamvakaki, V., Hatzimarinaki, M., Chaniotakis, N., 2008. Anal. Chem. 80, 5970–5975.

Wang, J., Liu, G.D., Lin, Y.H., 2006. Analyst 131, 477–483.

Wang, X.F., Zhou, Y., Xu, J.J., Chen, H.Y., 2009a. Adv. Funct. Mater. 19, 1–7.

Wang, Y., Lu, J., Tang, L.H., Chang, H.X., Li, J.H., 2009b. Anal. Chem. 81, 9710–9715.

Wang, Z.J., Zhou, X.Z., Zhang, J., Boey, F., Zhang, H., 2009c. J. Phys. Chem. C 113, 14071–14075.

Zhao, W., Sun, S.X., Xu, J.J., Chen, H.Y., Cao, X.J., Guan, X.H., 2008. Anal. Chem. 80, 3769–3776.

Zhou, M., Wang, Y.L., Zhai, Y.M., Zhai, J.F., Ren, W., Wang, F.A., Dong, S.J., 2009. Chem. Eur. J. 15, 6116–6120.

Zhu, C.Z., Guo, S.J., Fang, Y.X., Dong, S.J., 2010. ACS Nano 4, 2429–2437.